

Development of Nusselt number correlation using dimensional analysis for plate heat exchanger with a carboxymethyl cellulose solution

Karuppannan Muthamizhi · Ponnusamy Kalaichelvi

Received: 23 July 2013 / Accepted: 3 November 2014
© Springer-Verlag Berlin Heidelberg 2014

Abstract Versatile applications of plate heat exchangers (PHE's) in various industrial processes signify their command over other types of heat exchangers. The objective of this work was to derive Nusselt number correlations using dimensional analysis in terms of all the parameters to determine the heat transfer coefficients in a PHE for various concentrations of carboxymethyl cellulose (CMC) solution and it was also compared with the available models in literature. The heat transfer coefficient increases with increase in concentration of CMC from 0.1 to 0.6 %w/w and also increases with increase in mass flow rates of both cold and hot fluids from 0.016 to 0.099 kg/s. The Nusselt number correlation developed using dimensional analysis has predicted the Nusselt number for the given PHE with a RMS deviation of 14.61.

Abbreviations

PHE	Plate heat exchanger
CMC	Carboxymethyl cellulose
RTD	Resistance temperature detector

List of symbols

A_p	Effective plate heat transfer area (m ²)
c^*	Capacity ratio $c^* < 1$, dimensionless
F_T	Log-mean temperature difference correction factor, $0 < F_T < 1$ dimensionless
N_c	Number of channels
C_p	Specific heat of fluid at constant pressure (J/kg K)
D_h	Hydraulic diameter (m)
l	Plate length (m)

d	Port diameter (m)
C_s	Channel spacing (m)
h	Convective heat transfer coefficient (W/m ² K)
K	Fluid thermal conductivity (W/m K)
m	Mass flow rate (kg/s)
NTU	Number of transfer units
N_{Re}	Reynolds number, dimensionless
N_{Nu}	Nusselt number, dimensionless
N_{Pr}	Prandtl number, dimensionless
N_{Gr}	Grashoff number, dimensionless
Q	Rate of heat transfer (W)
T	Temperature (K)
ΔT	Temperature difference (K)
Δx	Plate thickness (m)
U_{exp}	Experimental overall heat transfer coefficient, including correction factor (W/m ² K)
U^*	Overall heat transfer coefficient (W/m ² K)
v	Velocity (m ² /s)
w	Width of the plate (m)
k	Consistency index (Pa s ⁿ)
n	Flow behavior index
K	Plate thermal conductivity (W/m K)
y	Dependent variable
a	Coefficient of x
x	Independent variable
b	Constant
i, j and k	Model parameters, dimensionless

Greek symbols

βg	Thermal expansion with acceleration due to gravity (*m/s ² K)
ρ	Density of the fluid (kg/m ³)
ΔT_{lm}	Logarithmic mean temperature difference (LMTD) (K)
ε	Exchanger thermal effectiveness

K. Muthamizhi · P. Kalaichelvi (✉)
Department of Chemical Engineering, National Institute of Technology, Tiruchirappalli 620015, Tamil Nadu, India
e-mail: kalai@nitt.edu

Subscripts

<i>h</i>	Hot
<i>c</i>	Cold
<i>i</i>	Fluid inlet
<i>o</i>	Fluid outlet
<i>ss</i>	Stainless steel
<i>max</i>	Maximum

1 Introduction

Gasketed PHE's are predominantly applied for liquid-to-liquid duty owing to their advantageous features such as very compact in design, easy to dismount for maintenance, cleaning or for modification of the heat transfer area by the addition or removal of plates [1]. The heat transfer surface area can be readily changed or rearranged due to the flexibility of the number of plates, plate type, and pass arrangements. The high turbulence due to plates reduces fouling to about 10–25 percent as that of a shell-and-tube exchanger. Indeed, leakage from one fluid to the other cannot take place unless a plate develops a hole. Since the gasket is between the plates, any leakage from the gasket is to the outside of the exchanger. Because of the high heat transfer coefficients, reduced fouling, absence of bypass and leakage streams, and pure counterflow arrangements, the surface area required for a PHE is 1/3–1/2 that of a shell-and-tube exchanger for a given heat duty. This would reduce the cost, overall volume, and maintenance space for the exchanger. Furthermore, the gross weight of a PHE is about only 1/6 as that of an equivalent shell-and-tube exchanger. The residence time of fluid particles on a given side is approximately the same for uniform heat applications such as sterilization, pasteurization, and cooking. In case of expensive fluids, a faster transient response and a better process control become inevitable. In this regard, there could be no significant hot or cold spots in the exchanger to avoid deterioration of heat sensitive fluids. PHE holds only a small volume of fluid with no hot or cold spots and thus is best suited for expensive fluids. High thermal performance can be well achieved in PHE's as the high degree of counterflow in PHE's makes even temperature approaches of up to 1 °C (2 °F) possible. Such a high thermal effectiveness (up to about 93 percent) facilitates economical low-grade heat recovery. Moreover, PHE's are devoid of flow-induced vibration, noise, high thermal stresses, and entry impingement problems, normally existing in shell-and-tube heat exchangers [2].

For the food industry, heat transfer studies in the PHE's with non-Newtonian fluid flow is of great importance, since various processes such as, cooling and heating of milk, citrus juices, and tropical fruit pulp pasteurization and concentration processes make use of PHE [3] and generally food fluids shows non-Newtonian flow behavior.

CMC, which is a non-Newtonian; a typical hydrocolloid imparts a pronounced effect on gel formation, water retention, and emulsifying and aroma retention with no direct influence on the taste and flavor of foodstuffs [4, 5]. CMC finds its applications as a stabilizer, binder, thickener, suspending and water-retaining agent, in ice-creams and frozen desserts, fluid and powdered fruit drinks, sauces and creams, cake mixes and slimming and dietary foods [6]. Hence different concentrations of CMC solution have been selected as working fluid for the present investigation.

Till date, a little research on the study of PHE with non-Newtonian fluids has been reported. Reilly and Tien [7] studied of natural convection heat transfer from heated vertical plate to a non-Newtonian fluid. For water–water duty, heat transfer and pressure drop studies in PHE is presented in articles [8–11]. Afonso et al. [12] conducted an experimental investigation to obtain a correlation for the determination of convective heat transfer coefficient in a PHE using yogurt as test fluid. Based on the experimental studies of Afonso et al. [12, 13], Fernandes et al. [14–18] has demonstrated numerical studies on PHE with yogurt as test fluid. Similar numerical studies in a PHE using egg yolk as test fluid were conducted by Gut et al. [19]. Jokar et al. [20] investigated the parameters that affect the two-phase heat transfer within the minichannel PHE's using refrigerant R-134a and developed appropriate correlations using dimensional analysis. Carezzato et al. [21] has also investigated the non-Newtonian heat transfer on a PHE with a generalized configuration, using CMC as a test solution. Lin et al. [22] developed a dimensionless correlation to characterize the heat transfer performance of the corrugated channel in a PHE using Buckingham pi theorem. Warnakulasuriya et al. [23] has established the correlation equations to predict the heat transfer and pressure drop of an absorbent salt solution in a commercial PHE. Mahdi et al. [24] developed a two-dimensional dynamic fouling model for milk fouling in a PHE. Cabral et al. [3] studied the thermo-physical (density) and flow properties (rheology) of pineapple juice in a PHE over a considerable range of temperature and soluble solid content to obtain a correlation for the determination of friction factor versus Reynolds number. Khan et al. [25] has been carried out experimental heat transfer studies with water–water in PHE for symmetric 30/30, 60/60, and mixed 30/60 chevron angle plates and a correlation to estimate Nusselt number as a function of Reynolds number, Prandtl number and chevron angle has been proposed. Pandey et al. [26] has investigated effects of nanofluid (Al_2O_3 in water 2, 3 and 4 vol%) and water as coolants on heat transfer, and pressure drop and exergy losses in PHE and has derived empirical correlation for Nusselt number and friction factor for both water and nanofluid. Correlations for the Nusselt number and the friction factor for 0.5 % aluminum oxide nanofluid in a PHE using Wilson plot method has developed by Dustin et al. [27]

and they have reported that the addition of 0.5 % aluminum oxide improve the convective and overall heat transfer coefficient as much as 11 and 4.85 % respectively.

Very few articles are available on the performance analysis of PHE's using non-Newtonian fluid for various concentrations and different flow rates in the literature. Researchers have used the dimensional analysis to develop Nusselt number correlation for PHE using fluids other than non-Newtonian fluid and for other geometries namely horizontal plate using non-Newtonian fluid as working fluid. However, none has used dimensional analysis to arrive at Nusselt number correlation for the combination of PHE and non-Newtonian fluid. Hence, the present study aimed to investigate the effects of flow rate and thermo-physical properties of CMC, a non-Newtonian fluid on the Nusselt number in the PHE of specific configuration and to derive a suitable correlation for Nusselt number from experimental data based on dimensional analysis. Least square method was applied to estimate the constants and the powers of the parameters involved in the developed correlation. Lastly, the developed Nusselt number correlation was validated with the experimental data points, and also compared with the available literature Nusselt number correlation.

2 Materials and methods

2.1 Experimental setup and procedure

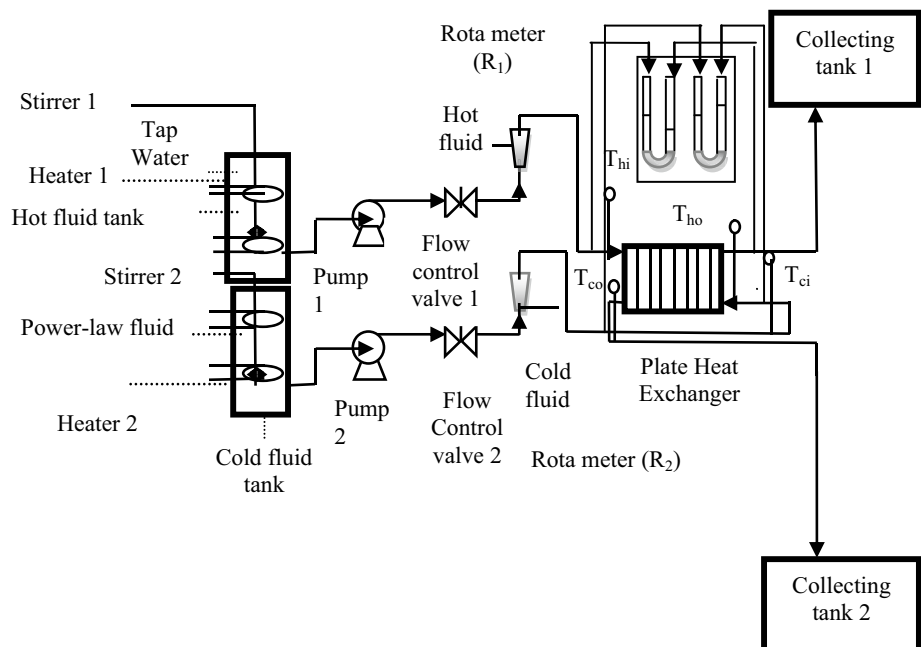
A six-channel corrugated type PHE with different flow rates and concentrations of working fluid CMC was used in the present study. The apparatus shown in Fig. 1 consisted of a

hot water storage tank, a cold fluid storage tank, immersed type of a pair of electrical heaters, a couple of liquid Rota meters, resistance temperature detectors, a manometer, two monoblock pumps and separate collection tank for cold fluid and hot water; which was recycled for reuse. A 25 litre capacity stainless steel tank for hot water storage was thermally well insulated to avoid heat loss to the atmosphere. Immersing type of electrical heaters of 2 kW capacity was fixed inside the hot water tank to raise the water temperature. A thermostat temperature controller with a range of 0–110 °C was connected with electrical heaters to set the temperature of hot water at a desired value.

Double pole on/off switch was connected with the 2 kW capacity electrical heaters. A monoblock type pump of 0.25 hp capacity was connected to the hot water storage tank to pump the hot water from the hot water storage tank to the PHE and a flow control valve in the same line was meant for regulating the flow. The cold fluid was stored in a separate stainless steel tank of equal capacity and well connected with another monoblock type pump of similar capacity used to pump cold fluid from cold fluid storage tank to PHE. A return flow line was provided to convey the cold fluid discharged at the outlet back into the collecting tank.

Two liquid Rota meters with accuracy of $\pm 2\%$ and measurement range of 0–10 LPM were well connected separately with the hot and the cold fluid lines to measure the fluid flow rate. These liquid flow meters were calibrated within their flow range. Four Resistance Temperature Detectors (RTDs) of model type: PT 100 was mainly used to measure the inlet and outlet temperature of each fluid with an accuracy of $\pm 0.1\text{ }^\circ\text{C}$. Out of the total four, two RTDs were separately placed at the inlet ports of both the fluids to measure the inlet

Fig. 1 Experimental setup of PHE



fluid temperature and remaining two RTDs were separately placed at the outlet ports of both the fluids to measure the outlet fluid temperature. Digital temperature indicators with channel selectors connected with RTDs displayed the output results of RTDs. These RTDs were calibrated within their temperature range via the corresponding calibration procedure. Table 1 shows the specifications of PHE.

CMC pure (food grade) was furnished by M/s. Merck. For a constant hot fluid mass flow rate and concentration of CMC, experimental data were collected for different flow rates of CMC solution (0.016–0.099 kg/s). Likewise, all runs were carried out for different concentrations (0.1–0.6 % w/w) and different hot fluid mass flow rates (0.016–0.099 kg/s) as detailed in the experimental plan shown in Fig. 2.

2.2 Data reduction for PHE with CMC

The heat load, Q , of a PHE, can be represented by Eq. (1a, b and c)

$$Q_h = m_h C_{p_h} (T_{hi} - T_{ho}) \quad (1a)$$

$$Q_c = m_c C_{p_c} (T_{co} - T_{ci}) \quad (1b)$$

$$Q = A_p U_{exp} \Delta T_{lm} F_T \quad (1c)$$

where $Q = Q_h = Q_c$, m is mass flow rate, C_p is specific heat of fluid, A is the effective PHE area, U_{exp} is the overall heat transfer coefficient, ΔT_{lm} is the logarithmic mean temperature difference and F_T is the correction factor [28].

$$\Delta T_{lm} = \frac{(T_{hi} - T_{co}) - (T_{ho} - T_{ci})}{\ln \left(\frac{T_{hi} - T_{co}}{T_{ho} - T_{ci}} \right)} \quad (1d)$$

$$A_p = lw \text{ (plate effective heat transfer area)} \quad (1e)$$

The correction factor F_T is a function of the exchanger configuration number of transfer units (NTU), defined in Eq. (3) and heat capacity ratio (c^* , defined in Eq. 4). For pure counter current flow ideal case, $F_T = 1$. For all other types of flow distribution, $0 < F_T < 1$. For the most usual configurations, researchers have utilized PHE simulation models to generate charts and tables in the form $F_T = F_T(NTU, c^*)$ or $\varepsilon = \varepsilon(NTU, c^*)$, where ε is the thermal effectiveness of the exchanger [29].

$$F_T = \begin{cases} \frac{1}{NTU(1-c^*)} \ln \left(\frac{1-c^*\varepsilon}{1-\varepsilon} \right) & \text{if } c^* < 1 \\ \frac{\varepsilon}{NTU-(1-\varepsilon)} & \text{if } c^* > 1 \end{cases} \quad (2)$$

$$NTU = \left(\frac{(N_c - 1)A_p U^*}{\min(m_h C_{p_h}, m_c C_{p_c})} \right) \quad (3)$$

$$\text{where } U^* = \frac{Q}{A \Delta T_{lm}}$$

Table 1 Specifications of PHE

Parameter	Value (m)
Plate thickness (Δx)	0.0008
Plate width (w)	0.125
Plate length (l)	0.425
Port diameter (d)	0.32
Channel spacing (C_s)	0.004

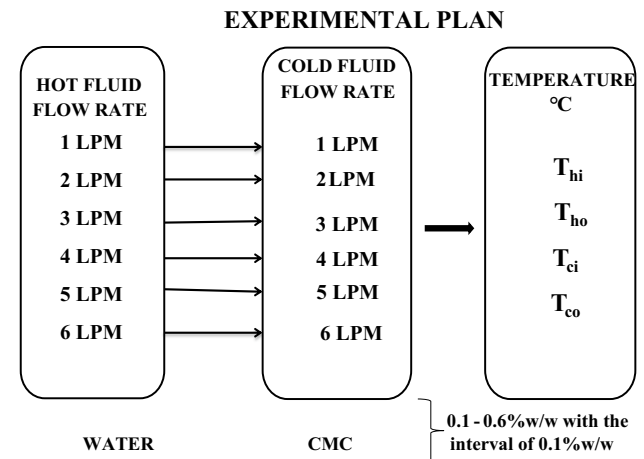


Fig. 2 Experimental plan

$$c^* = \left(\frac{\min(m_h C_{p_h}, m_c C_{p_c})}{\max(m_h C_{p_h}, m_c C_{p_c})} \right) \quad (4)$$

$$\varepsilon = \frac{Q}{Q_{max}} \quad (5)$$

where $Q_{max} = \min(m_h C_{p_h}, m_c C_{p_c})(T_{hi} - T_{ci})$

F_T is calculated using Eq. 2 incorporating Eqs. (3, 4 and 5) in Eq. 2. Q_h and Q_c heat load are calculated using Eq. (1a, b), then these values F_T , ΔT_{lm} , Q , A_p are used to calculate U_{exp} values using Eq. (1c).

After the determination of U_{exp} in Eq. (1c), the convective coefficient of the water side h_h of the PHE was obtained using same flow analysis as described by Vlasogiannis et al. [30]. Introducing pure water as the cold fluid and hot fluid as well, ($h_h = h_c$) the exchanger was first tested in a single-phase operation. To extract an accurate correlation for the hot fluid side heat transfer coefficient of the available PHE, a series of measurements were analyzed by the variant of the modified Wilson plot technique.

$$\frac{1}{U_{exp}} = \frac{1}{h_h} + \frac{1}{h_c} + \frac{\Delta x}{K_{ss}} \quad (6)$$

Calculated h_h was again substituted in Eq. 6 to predict cold side heat transfer coefficient (h_c) where Δx is the plate

thickness and k_{ss} is the thermal conductivity of the plate material (stainless steel) [30].

The correlation whose general form presented in Eq. (7) is commonly used for Newtonian fluids under turbulent flow, where Nusselt number, Reynolds number and Prandtl number (Nu, Re and Pr respectively) are dimensionless numbers and i, j , and k are empirical parameters [2].

$$N_{Nu} = iN_{Re}^j N_{Pr}^k \quad (7)$$

A better additive has to be selected using the rheological parameters as the criteria for selection in order to best serve the food industry. Typical rheological parameters, consistency index, which is a strong function of the concentration of the solution and temperature, and flow index, which does not have a strong dependence on the concentration and temperature of the solution are used in the power-law model [31].

CMC commonly used as a stabilizer, thickener, gelling agent or emulsifier due to its rheological properties could be well represented by the power-law model. Generalized equations of Reynolds number and Prandtl number for non-Newtonian fluid are presented in Eqs. (8 and 9) [32].

$$N_{Re} = \left(\frac{\rho v^{2-n} D_h^n}{k} \right) \quad (8)$$

$$N_{Pr} = \left(\frac{k C_p \left(\frac{v}{D_h} \right)^{n-1}}{K} \right) \quad (9)$$

In these equations, N_{Pr} , ρ , v , D_h , K , N_{Re} and C_p are Prandtl Number, density, the average velocity of the fluid, hydraulic diameter, thermal conductivity, Reynolds Number and heat capacity respectively, and k and n are the rheological parameters, consistency index and power law index of the CMC solution respectively.

2.3 Development of Nusselt number correlation based on dimensional analysis

Dimensional analysis is the mathematical technique of deriving relations between physical quantities by identifying their dimensions. The dimension of any physical quantity is a combination of the basic physical dimensions that compose it. Length L, mass M, Temperature T, Heat Hand time t are fundamental dimensions, all physical quantities are expressed in terms of these fundamental dimensions. Whenever it is possible to identify the factors involved in a physical situation, dimensional analysis forms a relationship between them. Manjula et al. [33] have developed a correlation for mixing time of the jet mixer using

dimensional analysis. The heat transfer rate (Q , W) per unit area (A , m^2) in PHE depends upon the parameters such as Hydraulic diameter (D_h , m) of PHE, velocity (v , m/s), density (ρ , kg/m^3), specific heat (C_p , $J/kg K$), thermal expansion with gravitational force (βg , $m/s/t$), thermal conductivity (K , $W/m K$), flow behavior index (n), consistency index (k , $Pa s^n$), temperature difference (ΔT , K) etc. of non-Newtonian fluid. For dimensional analysis, the dependencies of these variables have been grouped together as follows

$$\frac{Q}{A} (v, \rho, \beta g, \Delta T, K, k, n, C_p, D_h) = 0 \quad (10)$$

In the present study, the number of variables involved in the process was more than the number of fundamental dimensions, so the Buckingham method was considered. This theorem states that the relationship between r variables is expressed as a relationship between $r - s$ non-dimensional groups of variables (called π groups), where s is the number of fundamental dimensions required to express the r variables. In Eq. (10), there were 10 variables present and all the variables were expressed in terms of the five basic fundamental dimensions (s), thus $r = 10$, $s = 5$. The number of π groups that were formed was $r - s = 10 - 5 = 5$ but as n was already $M^0 L^0 T^0$, dimensionless groups were reduced to 4, $f(\pi_1, \pi_2, \pi_3, \pi_4) = 0$. As the π groups were all dimensionless, i.e. $M^0 L^0 T^0$, the principle of dimensional homogeneity was used to equate the dimensions for each π group. Hence, the following expression of heat transfer coefficient in terms of Nusselt number was obtained

$$Nu = f \left(\left(\frac{U}{D^{\frac{n}{n-2}} \rho^{\frac{1}{n-2}}} \right) \left(\frac{cp}{D^{\frac{2-2n}{n-2}} \rho^{\frac{1-n}{n-2}} K} \right) \left(\frac{\Delta T \beta g}{D^{\frac{n+2}{n-2}} \rho^{\frac{2}{n-2}}} \right) \right) \quad (11)$$

Equation (11) shows the relation between the Nusselt number and all the possible variables that could affect heat transfer in the PHE considered for the present study.

3 Results and discussion

In the present study, a six-channel corrugated type PHE with working fluid CMC was used. The effects of concentrations and flow rates of both the hot and cold fluids on Nusselt number were analyzed based on the experimental data, and were discussed below.

3.1 Effect of cold fluid mass flow rate on heat transfer coefficient

To study the effect of cold fluid mass flow rate on the heat transfer coefficient obtained experimentally for PHE, values of heat transfer coefficient were plotted against

different flow rates of cold fluid at various concentrations of CMC while maintaining a constant hot fluid flow rate of 0.099 kg/s, as shown in Fig. 3.

It is observed from Fig. 3 that the heat transfer coefficient has increased with the increase in cold fluid mass flow rate from 0.016 to 0.099 kg/s as well as for 0.1, 0.3 and 0.5 % w/w concentrations of CMC at a hot fluid mass flow rate of 0.099 kg/s. The same was observed for 0.2, 0.4 and 0.6 % w/w concentrations of CMC and 0.016–0.083 kg/s of hot fluid mass flow rate. The increase in the values of the heat transfer coefficients in the aforementioned cases could be attributed to the increase in flow rates as well as turbulence.

Thermo-physical properties like thermal conductivity, density, flow behaviour index, consistency index and specific heat depended on temperature and concentration of CMC solution. As the concentration of CMC increased, the thermal conductivity of CMC decreased while, the ratio of dry CMC mass to water quantity increased. This restricted the movement of the CMC solution and water, thus the ability of CMC to conduct heat, represented by thermal conductivity also decreased. As carbohydrate CMC granule was the principal solid content of CMC its concentration directly affected the density of CMC. As a result of increase in concentration, mass of the CMC granules and density of the CMC solution also increased [34].

An increase in the concentration of a dissolved or dispersed substance of CMC solution generally gives rise to an increased viscosity, as does increasing the molecular weight of a solute of CMC solution and the specific heat also increases, when concentration increases. Congruently, it was evident from the developed correlation that the heat transfer coefficient was directly proportional to the properties such as density, specific heat and viscosity and inversely proportional to thermal conductivity. This implied that the heat transfer coefficient would also increase with an increase in concentration, validating the results shown in Fig. 3.

3.2 Effect of hot fluid mass flow rate on heat transfer coefficient

In order to analyze the effect of hot fluid mass flow rate on the heat transfer coefficient, a graph was plotted between the heat transfer coefficient and the hot fluid flow rate for different cold fluid flow rates and a particular concentration of CMC (0.6 % w/w), as illustrated in Fig. 4.

As the flow rate increases, driving force also increases, so it is inferred from Fig. 4 that the convective heat transfer coefficient has increased with the increase in hot fluid mass flow rates from 0.016 to 0.099 kg/s, for 0.6 % w/w concentration of CMC and for cold fluid mass flow rate 0.016, 0.055 and 0.083 kg/s. The same was observed for 0.1–0.5 % w/w concentrations of CMC and for 0.033, 0.066 and 0.099 kg/s cold fluid mass flow rate.

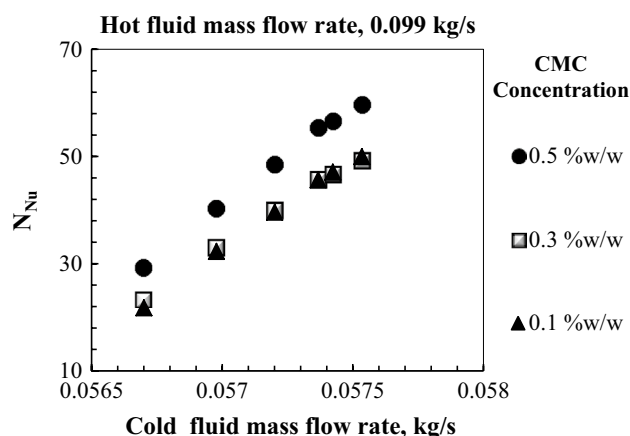


Fig. 3 The effect of cold fluid mass flow rate on heat transfer coefficient for 0.099 kg/s hot fluid mass flow rate

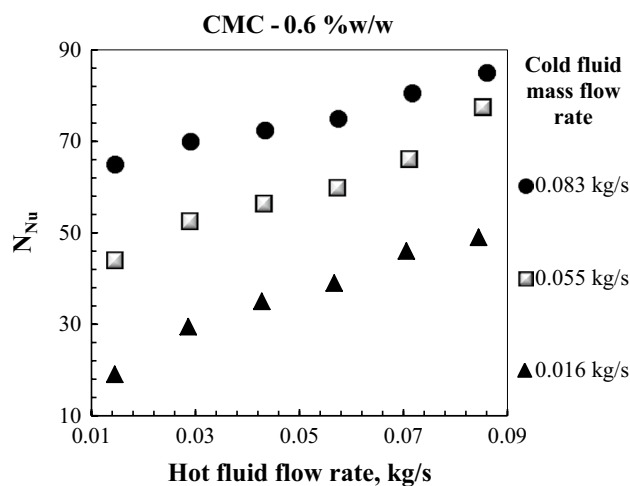


Fig. 4 The effect of hot fluid mass flow rate on the heat transfer coefficient of 0.6 % w/w CMC

3.3 Estimation of powers in the Nusselt number correlation using experimental data

LINEST (Excel tool function) was used to determine the significance of the effect of each variable involved in the equation of Nusselt number. The LINEST function calculates the statistics for a line by using the least squares method to calculate a straight line that best fits your data, and then returns an array that describes the line. Equation (11) can be rewritten by taking logarithm on both sides of the equation.

$$\log Nu = a_1 \log \left(\frac{U}{D^{\frac{n}{n-2}} \rho^{\frac{1}{n-2}}} \right) + a_2 \log \left(\frac{cp}{D^{\frac{2-2n}{n-2}} \rho^{\frac{1-n}{n-2}} K} \right) + a_3 \log \left(\frac{\Delta T \beta g}{D^{\frac{n+2}{n-2}} \rho^{\frac{2}{n-2}}} \right) + b \quad (12)$$

Table 2 Comparison of experimental Nusselt number of CMC-0.1 % w/w with the literature correlation and developed correlation

S. no.	Correlation	Working fluid and configuration	Equation	RMS deviation
1.	Developed correlation	CMC No. of plates: 7	13	14.61
2.	Afonso et al. [12]	Yogurt No. of plates: 15, 13, 11, 7 and 5	14	18.57
3.	Fernandes et al. [16]	Yogurt No. of plates: 15, 13, 11, 7 and 5	15a 15b 15c	16.26 26.03 18.44

Equation (12) is in the form of $y = ax + b$, where y is the dependent variable which is a function of the independent variable, x is the independent variable, a is the coefficient of x and b is a constant. In the present study, Eq. (12) was fitted to the experimental data points. Least square method has been used to calculate the coefficients of the equation in Nusselt number which gives the best fit to experimental data points. Equation (12) was reduced to the following form:

$$Nu = 0.415834 \left(\left(\frac{U}{D^{\frac{n}{n-2}} \rho^{\frac{1}{n-2}}} \right)^{0.651139} \times \left(\frac{cp}{D^{\frac{2-2n}{n-2}} \rho^{\frac{1-n}{n-2}} K} \right)^{2.267862} \left(\frac{\Delta T \beta g}{D^{\frac{n+2}{n-2}} \rho^{\frac{2}{n-2}}} \right)^{-0.15291} \right) \quad (13)$$

Root Mean Square (RMS) deviation between the experimental Nusselt Number and Nusselt number estimated using the correlation (Eq. 13) was 14.61.

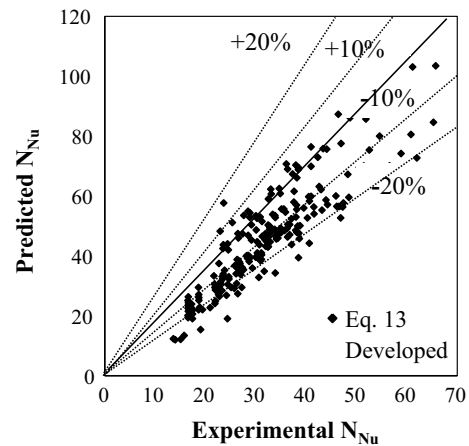
3.4 Comparison of the developed Nusselt number correlation with the Nusselt number correlation available in literature

The experimental Nusselt number was calculated for PHE with CMC using Eqs. (1–6) and it was compared with the Nusselt number correlation developed by Afonso et al. [12] (Eq. 14) and Fernandes et al. [16] (Eq. 15a, b, c). Model equations proposed by Afonso et al. [12] (Eq. 14) and Fernandes et al. [16] are for stirred yogurt which is a non-Newtonian fluid of shear-thinning type. Since CMC also comes under the same category, the experimental Nusselt number calculated in the present study are compared with Nusselt number calculated using the Nusselt number correlation proposed by Afonso et al. [12] (Eq. 14) and Fernandes et al. [16].

$$Nu = 1.759Re^{0.455}Pr^{0.3} \quad (14)$$

$$Nu = 1.878Re^{0.463}Pr^{0.3}; R^2 = 0.985 \quad (15a)$$

$$Nu = 1.809Re^{0.347}Pr^{0.3}; R^2 = 0.993 \quad (15b)$$

**Fig. 5** Experimental N_{Nu} versus predicted N_{Nu} using Eq. (10)

$$Nu = 1.808Re^{0.449}Pr^{0.3}; R^2 = 0.987 \quad (15c)$$

Here R^2 is coefficient of determination. This experimental Nusselt number was compared with the Nusselt number obtained using literature correlations as well as correlation developed in the present study and the RMS deviations have been presented in Table 2.

The RMS deviation calculated for Nusselt numbers obtained using Afonso et al. [12] and Fernandes et al. [16] correlations have shown more variations when compared to the developed correlation as a result of usage of different configurations and fluids and Fig. 5 compares the experimental N_{Nu} with those predicted from Eq. (13) and RMS deviation varies between -20 and $+20$ %. From the variations of the exponents in Eqs. (6) and (13), it can be inferred experimental N_{Nu} and predicted N_{Nu} are affected by the factors listed in Eq. (10), respectively [22].

3.5 Uncertainty analysis in PHE

The objective of well designed experiments is to minimize the error. Uncertainty is a measure of repeatability of experiment and needed to prove the accuracy of the experiments. The errors are based on the least counts and the sensitivities of the measuring instruments used in the

Table 3 The average possible error for the experimental parameters

S. no.	Basic equation	Uncertainty equation	Uncertainty %
1.	$N_{Re} = \left(\frac{\rho v^{2-n} D_h^n}{k} \right)$	$\frac{\Delta Re}{Re} = \left\{ \left(\frac{\Delta D_h}{D_h} \right)^2 + \left(\frac{\Delta m}{m} \right)^2 \right\}^{0.5}$	1.98
2.	$F_T = \left\{ \frac{1}{NTU(1-C^*)} \ln \left(\frac{1-C^*\epsilon}{1-\epsilon} \right) \right\}$ if $C^* < 1$	$\frac{\Delta f}{f} = \left\{ \left(\frac{\Delta T_{hi}}{T_{hi}} \right)^2 + \left(\frac{\Delta T_{ho}}{T_{ho}} \right)^2 + \left(\frac{\Delta T_{ci}}{T_{ci}} \right)^2 + \left(\frac{\Delta T_{co}}{T_{co}} \right)^2 \right\}^{0.5}$	2.30
3.	$\epsilon = \frac{Q}{\min(m_h C_{ph}, m_c C_{pc}(T_{hi} - T_{ci}))}$	$\frac{\Delta \epsilon}{\epsilon} = \left\{ \left(\frac{\Delta T_{hi}}{T_{hi}} \right)^2 + \left(\frac{\Delta T_{ho}}{T_{ho}} \right)^2 + \left(\frac{\Delta T_{ci}}{T_{ci}} \right)^2 \right\}^{0.5}$	0.41
4.	$\frac{1}{U_{exp}} = \frac{1}{h_c} + \frac{1}{h_h} + \frac{\Delta x}{k_{ss}}$	$\frac{\Delta h_c}{h_c} = \left\{ \left(\frac{\Delta U_{exp}}{U_{exp}} \right)^2 + \left(\frac{\Delta h_h}{h_h} \right)^2 + \left(\frac{\Delta x}{x} \right)^2 \right\}^{0.5}$	1.78
5.	$Nu = \frac{h_c D_h}{K}$	$\frac{\Delta Nu}{Nu} = \left\{ \left(\frac{\Delta h_c}{h_c} \right)^2 + \left(\frac{\Delta D_h}{D_h} \right)^2 \right\}^{0.5}$	1.75

present investigation. The detailed systematic error analysis is made in the present study to estimate the error associated with experimentation as given Table 3.

4 Conclusion

Experimental analysis of the heat transfer in PHE using CMC as a working cold fluid and development of Nusselt number correlation using dimensional analysis leads to the following conclusions.

1. The heat transfer coefficient has increased as the concentration of CMC increased from 0.1 to 0.6 % also an increase in mass flow rates of both cold and hot fluids from 0.016 to 0.099 kg/s as depicted an increase in the heat transfer coefficient.
2. The correlation developed using dimensional analysis has predicted the Nusselt number for the given PHE with a RMS deviation of 14.61.

$$Nu = 0.415834 \left(\left(\frac{U}{D^{\frac{n}{n-2}} \rho^{\frac{1}{n-2}}} \right)^{0.651139} \left(\frac{cp}{D^{\frac{2-2n}{n-2}} \rho^{\frac{1-n}{n-2}} K} \right)^{2.267862} \right) \times \left(\frac{\Delta T \beta g}{D^{\frac{n+2}{n-2}} \rho^{\frac{2}{n-2}}} \right)^{-0.15291}$$

Nusselt numbers obtained using correlations proposed by Afonso et al. [12] and Fernandes et al. [16] revealed RMS deviation values greater than 14.61.

3. However, validity of the correlation developed can be further improved, making use of a larger number of experimental data points, covering a wider range of parameters and non-Newtonian fluids.

Acknowledgments The authors wish to express their appreciation to Council of Scientific and Industrial Research (CSIR) for the

financial support given for carrying out this investigation (Ref. No. 22/514/10-EMR-II).

References

1. Focke WW, Zachariades J, Olivier I (1985) The effect of the corrugation inclination angle on the thermo hydraulic performance of PHEs. *Int J Heat Mass Transf* 28:1469–1497
2. Shah RK, Focke WW (1988) Plate heat exchangers and their design theory. In: Shah RK, Subbarao EC, Mashelkar RA (eds) *Heat transfer equipment design*. Hemisphere, Washington, pp 227–254
3. Cabral RAF, Gut JAW, Telis VRN, Romero TJ (2010) Non-Newtonian flow and pressure drop of pineapple juice in a PHE. *Braz J Chem Eng* 27(4):563–571
4. Carr JM (1993) Hydrocolloids and stabilizers. *Food Technol* 47(10):100
5. Hegedusi V, Herceg Z, Rimac S (2000) Rheological properties of carboxymethylcellulose and whey model solutions before and after freezing. *Food Technol Biotechnol* 38(1):19–26
6. Speers RA, Tung M A (1986) Concentration and temperature dependence of flow behavior of xanthan gum dispersions. *J Food Sci* 51(1):96–98
7. Reilly IG, Tien C, Adelman M (1965) Experimental study of natural convective heat transfer from a vertical plate in a non-Newtonian fluid. *Can J Chem Eng* 43(4):157–160
8. Cooper A (1974) Recover more heat with plate heat exchangers. *Chem Eng* 285:280–285
9. Clark DF (1974) Plate heat exchanger design and recent development. *Chem Eng* 285:275–279
10. Edwards MF, Changal Vaie AA, Parrott DL (1974) Heat transfer and pressure drop characteristics of a plate heat exchanger using Newtonian and non-Newtonian liquids. *Chem Eng* 285:286–288
11. Marriott J (1971) Where and how to use plate heat exchangers. *Chem Eng* 78:127–134
12. Afonso IM, Maia L, Melo LF (2003) Heat transfer and rheology of stirred yoghurt during cooling in plate heat exchangers. *J Food Eng* 57:179–187
13. Afonso IM, Cruz P, Maia JM, Melo LF (2008) Simplified numerical simulation to obtain heat transfer correlations for stirred yoghurt in a plate heat exchanger. *J Food Eng* 86(4):296–303
14. Fernandes CS, Dias RP, Nobrega JM, Maia JM (2005) Effect of corrugation angle on the hydrodynamic behaviour of power-law fluids during a flow in plate heat exchanger. In: Shah RK, Ishizuka M, Rudy TM, Wadekar VV (eds) *Proceedings of the fifth international conference on enhanced, compact and ultra compact*

- heat exchangers: science engineering and technology, Engineering Conferences International, USA
15. Fernandes CS, Dias RP, Nobrega JM, Afonso IM, Melo LF, Maia JM (2005) Simulation of stirred yoghurt processing in plate heat exchangers. *J Food Eng* 69:281–290
 16. Fernandes CS, Dias RP, Nobrega JM, Afonso IM, Melo LF, Maia JM (2006) Thermal behaviour of stirred yoghurt during cooling in plate heat exchangers. *J Food Eng* 76:433–439
 17. Fernandes CS, Dias RP, Nobrega JM, Maia JM (2007) Laminar flow in chevron-type plate heat exchangers: CFD analysis of tortuosity, shape factor and friction factor. *Chem Eng Process* 46:825–833
 18. Fernandes CS, Dias RP, Nobrega JM (2008) Maia friction factors of power-law fluids in chevron-type plate heat exchangers. *J Food Eng* 89:441–447
 19. Gut JAW, Pinto JM, Gabas AL, Romer JT (2003) Pasteurization of egg yolk in plate heat exchangers thermo-physical properties and process simulation, Annual meeting, CA 123:16–21
 20. Jokar A, Hosni M, Mohammad H, Eckels SJ (2006) Dimensional analysis on the evaporation and condensation of refrigerant R-134a in minichannel plate heat exchangers. *Appl Therm Eng* 26(17–18):2287–2300
 21. Carezzato A, Alcantara MR, Romero TJ, Tadini CC, Gut JAW (2007) Non-Newtonian heat transfer on a plate heat exchanger with generalized configurations. *Chem Eng Technol* 30(1):21–26
 22. Lin JH, Huang CY, Su CC (2007) Dimensional analysis for the heat transfer characteristics in the corrugated channels of plate heat exchangers. *Int Commun Heat Mass Transf* 34(3):304–312
 23. Warnakulasuriya FSK, Worek WM (2008) Heat transfer and pressure drop properties of high viscous solutions in plate heat exchangers. *Int J Heat Mass Transf* 51:52–67
 24. Mahdi Y, Mouheb A, Oufer L (2009) A dynamic model for milk fouling in a plate heat exchanger. *Appl Math Model* 33:648–662
 25. Khan TS, Khan MS, Chyu MC, Ayub ZH (2012) Experimental investigation of single phase convective heat transfer coefficient in a corrugated plate heat exchanger for multiple plate configurations. *Appl Therm Eng* 30:1058–1065
 26. Pandey SD, Nema VK (2012) Experimental analysis of heat transfer and friction factor of nanofluid as a coolant in a corrugated plate heat exchanger. *Exp Thermal Fluid Sci* 38:248–256
 27. Ray DR, Das DK, Vajjha RS (2014) Experimental and numerical investigations of nanofluids performance in a compact minichannel plate heat exchanger. *Int J Heat Mass Transf* 71:732–746
 28. Rohsenow WM, Hartnett JP, Cho YI (1998) Handbook of heat transfer, 3rd edn. McGraw-Hill, New York
 29. Gut JAW, Fernandes R, Pinto JM, Tadinia CC (2004) Thermal model validation of plate heat exchangers with generalized configurations. *Chem Eng Sci* 59:4591–4600
 30. Vlasogiannis P, Karagiannis G, Argyropoulos P, Bontozoglou V (2002) Air–water two-phase flow and heat transfer in a plate heat exchanger. *Int J Multiph Flow* 28:757–772
 31. Wanchoo RK, Sharma SK, Bansal R (1996) Rheological parameters of some water-soluble polymers. *J Polym Mater* 13:49–55
 32. Moradi M, Etemad SG, Moheb A (2006) Laminar flow heat transfer of a pseudoplastic fluid through a double pipe heat exchanger. *Iran J Chem Eng* 3(2):13–19
 33. Manjula P, Kalaichelvi P, Dheenathayalan K (2009) Development of mixing time correlation for a double jet mixer. *J Chem Technol Biotechnol* 85(1):115–120
 34. Sopa C, Cumnueng W, Thavachai T, Juntanee U, Jatuphong V (2008) Effects of temperature and concentration on thermal properties of cassava starch solutions. *Songklanakarin J Sci Technol* 30(3):05–411